ELSEVIER

Thermochimica Acta 384 (2002) 315–328

thermochimica acta

www.elsevier.com/locate/tca

A combinatorial approach to surface contacts in solid phase reactions

Christiaan Richter, Hendrik J. Viljoen*

Department of Chemical Engineering, University of Nebraska, Lincoln, NE 68588-0126, USA

Abstract

Macro-kinetic models for solid phase reactions require information about the contact area between reactants. A classical probability is presented to calculate the expectancy value for contact between two specified species when three different solid phases are present in the system. Consider the generic reaction $a\mathrm{A(s)} + b\mathrm{B(s)} \rightarrow c\mathrm{C(s,g)}$ (if C is volatile the two-phase problem results). The expectancy value depends on the surface area densities $\sigma_i = N_i v$ where N_i denotes the particle density of species i and v_i is the volume per particle—instead of using distributions, the analysis is based on average particle sizes. To include the important role of particle geometry, the reactants are modeled as rectangular rhombi. The differences in reaction rate are investigated for cubes (quasi-spheres), platelets and needles by adjusting the aspect ratios. As the reaction proceeds reactants are consumed and products form that change the probabilities for reactant contacts. The evolution of particle sizes must be tracked and mechanisms that affect particle sizes must be included in the model. The dimensions change with reaction, compression and fracture. Fracture is described by the Hiramatsu–Oko equation that relates bed pressure with an equilibrium dimension. The particle size of the (solid) product depends specifically on the reaction mechanism. To illustrate the combinatorial approach, it is applied to a mechanism where C desorbs from the A/B interface, but then it either nucleates to form C particles or adsorbs on existing C particles. Factors that influence the reaction rate are initial particle sizes, aspect ratios, fracture criteria and stoichiometry.

Keywords: Combinatorics; Surface contacts; Solid phase reactions

1. Introduction

Rate expressions formulated for gas or liquid reactions are invariably of the form $f(T,P)g([\mathrm{C_A}], [\mathrm{C_B}], \ldots)$, like the familiar expression $r = k_0\, \mathrm{e}^{-E/RT}\, g([\mathrm{C_A}], [\mathrm{C_B}], \ldots)$. These expressions are justified by experiments and/or various theories. When the reactants are solids many of the theoretical arguments lose their applicability. It is quite obvious that usage of concentrations is not acceptable, but surface areas are important variables. Although descriptions for gas–solid reactions have recognized the importance of changing surface area, going all the way back to the shrinking-core model Smith [1] solid–solid reaction models have not included particle contacts, geometry and evolution of size to a reasonable level of sophistication.

Tamhankar and Doraiswamy [2] reviewed different solid–solid models. Based on the rate limiting process, models have been proposed to account for product layer diffusion, nucleation growth and kinetically controlled reactions. Particle geometries of spheres, discs and cubes have been considered. In most of these models the conversion is expressed as a function of time and in

* Corresponding author. Tel.: +1-402-472-9318; fax: +1-402-472-6989.
E-mail address: chrdhjv@engunx.unl.edu (H.J. Viljoen).

0040-6031/02/$ – see front matter
PII: S0040-6031(01)00788-2

some models additional variables are included to account for the change in volume due to reaction. During the past three decades there has been an increasing interest in combustion synthesis as an alternative route to manufacture carbides, nitrides, intermetallics and oxides [3]. Merzhanov presents several mechanisms that further underscore the complexities of some of these mechanisms. For example, pure Mo and B does not react, but powders with small amounts of oxides react readily. Volatile sub-oxides form and act as carriers of reactants to reaction sites on other solids. Models have been developed for solid–solid and solid–liquid reactions and a further distinction between microscopic models and macroscopic models can be made. These different models have been reviewed by Varma et al. [4]. But an important deficiency of macroscopic models remains the limited number of models that have recognized the role of surface area contacts.

There are three factors that determine the rate of the solid–solid reaction $a\mathrm{A(s)} + b\mathrm{B(s)} \rightarrow c\mathrm{C}$: the concentration of A and B atoms that could interact, the fraction of them that has sufficient energy and the frequency of interacting events. Only surface atoms can participate in the reaction but surface contacts between particles of the same species or contact with the product (if C is condensed) reduce this number. The expectancy to have an A/B contact instead of A/A, B/B, A/C and B/C is best described by a classical probability approach. In order to track the total surface area of the species, it is necessary to follow the evolution of their particle sizes. In most theoretical descriptions the particles are assumed to be spherical. This assumption may be convenient but not necessarily the best. When only one variable is used to describe the physical state of the particle, it is not possible to distinguish between spheres, needles and platelets. The simplest way to account for aspect ratios is to assume a rhombohedral form. The dynamics of particle size and shape is resolved by tracking the changes in the three principal dimensions. As is the case in many solid phase reactions, the product may be a solid that forms an intermediate layer between reactants, quickly transforming the rate to a diffusion-controlled process. The particle size of the product also becomes an issue if C is a solid. Since product layers could form on A and B, it competes with A/B contacts and has a major effect on the overall kinetics. Clearly the reaction mechanism plays a very important role. If C remains solid immediately after its formation, the system may become diffusion-controlled. If C is volatile when it first forms and then condenses as particles the product will interfere with A/B contacts in a different way.

Mechanical effects are largely neglected in solid–solid reactions. This may be quite reasonable for many cases, but solid phase reactions in the presence of mechanical loading become dynamically more complex due to the added possibility of particle deformation and fracture. An important stimulus for this work has stemmed from the fascinating results of Enikolopyan and co-workers. They studied many systems, both endothermic and exothermic in Bridgman anvils and high-pressure extruders [5–13]. Thermite mixtures of Al and Fe_2O_3, pressed into discs of thickness 4 mm, reacted completely within 100 ns [10,12]—the anvil was destroyed and the lack of plastic deformation in its fracture zones points to a detonation. Particles were ejected from cylindrical pre-forms (samples were not radially contained) at velocities up to 2000 m/s [9]. Reactions were accompanied by the emission of light, high-energy electrons and acoustic emission. These experiments lend further proof to the existence of structural collapse of reactants during the course of the reaction. There is a continuing effort to initiate and sustain chemical reactions by dynamic loading, most notably is the work of Nesterenko and Meyers [14–16] and their co-workers. Other important contributions in this regard have been made by Thadhani [17,18], Krueger et al. [19], Boslough [20], Johnson et al. [21], Bennett et al. [22,23], Vreeland et al. [24] and Horie and Kipp [25]. One must distinguish these efforts from the Enikolopyan experiments in the way that mechanical loading is accomplished. When flyer plates, shock waves (from external explosive origin) or high velocity impact of reactive pellets are employed, transfer of energy occurs across a thin layer at the shock front. The energy is transferred from kinetic energy to thermal energy, elastic potential energy and plastic deformation. In hydrostatic experiments, the whole system is in an elevated energy state due to added elastic potential energy. Transfer of energy occurs from elastic to thermal and kinetic modes.

Fracture generates new surface and it accelerates the reaction rate. In shock conditions variations in local particle velocities could re-arrange particle contacts, in other words mixing is not an event that

precedes reaction but occurs during reaction. The probability for A/B contacts must be determined whilst the A, B and C surface areas are changing. Chemical reaction and fracture are not the only factors that change particle dimensions. Under conditions of high-pressures particles can also be compressed.

No new solid–solid reaction mechanisms are proposed in this study. But the main contribution is the use of combinatorics to determine the expectancy value for certain surface contacts. The method is applied to different mechanisms. Mechanical loading is also considered in some examples and the effects of fracture and compression are included.

2. Mathematical model

Consider a sample of solid powders compressed so that there are no pores left, i.e. all points on the surface of any given particle are in contact (associated/paired) with a unique point other than itself.[1] It is further assumed that the powders are 'ideally mixed'. This means that any point x on any surface has no greater inherent affinity (probability) to be in contact with any other point y rather than a third point z.[2] One can physically interpret this ideal limit as the limit where *the effects of particle shape and size* in preferring a particular packing or pattern of contacts *are minimized*. The larger the number of particles will be, the more correct this approach will be.

The generic reaction $\mathrm{A(s)} + \mathrm{B(s)} \rightarrow \mathrm{C(s/g)}$ can form either a gaseous or a solid product and we consider both possibilities. A liquid product is not included in the current analysis. First we need to model the particles.

2.1. Model of particle

All particles are assumed to be rectangular rhombi. Consider species A and let d_A denotes a scaled[3] Bohr radius such that the volume of one A atom $= d_\mathrm{A}^3$. The three principal dimensions of a rhombus can be expressed in terms of multiples of d_A as follows: $(X_\mathrm{A}, Y_\mathrm{A}, Z_\mathrm{A}) = d_\mathrm{A}(K_\mathrm{A}, L_\mathrm{A}, M_\mathrm{A})$. The fraction of atoms in the particle that occupy surface sites is $2[K_\mathrm{A}L_\mathrm{A}+K_\mathrm{A}M_\mathrm{A} + M_\mathrm{A}L_\mathrm{A} - 2(K_\mathrm{A} + L_\mathrm{A} + M_\mathrm{A}) + 4]/K_\mathrm{A}L_\mathrm{A}M_\mathrm{A}$. The surface area can also be expressed in units of the scaled Bohr radius.

$$S_\mathrm{A} = 2[K_\mathrm{A}L_\mathrm{A} + L_\mathrm{A}M_\mathrm{A} + K_\mathrm{A}M_\mathrm{A}] \tag{1}$$

The other surface areas S_B and S_C are defined similarly. The particle size distribution of species A is given by $f_\mathrm{A}(\bar{x}, t)$ and $f_\mathrm{A}(\bar{x}, t)\,\mathrm{d}k\,\mathrm{d}l\,\mathrm{d}m$ is the number of particles with dimensions between K_A and $K_\mathrm{A} + \mathrm{d}k$, L_A and $L_\mathrm{A} + \mathrm{d}l$, M_A and $M_\mathrm{A} + \mathrm{d}m$ at the position $\bar{x}$ in the reactor bed at time t. In order to make the further derivation tractable, we will not use a distribution but an average particle size $P_\mathrm{A}(K_\mathrm{A}, L_\mathrm{A}, M_\mathrm{A}, \bar{x}, t)$. Also define $N_\mathrm{A}(\bar{x}, t)$ as the number of particles of species A per unit volume of reactor bed. If the material density of species A is ρ_A, then the bed density of A at a point in the reactor is given by

$$\rho_\mathrm{BA} = N_\mathrm{A}K_\mathrm{A}L_\mathrm{A}M_\mathrm{A}d_\mathrm{A}^3\rho_\mathrm{A} \tag{2}$$

Likewise we can define the surface area of A per unit volume of bed at a specific point in space and time in terms of multiples of d_A^2 it is

$$\sigma_\mathrm{A} = 2N_\mathrm{A}[K_\mathrm{A}L_\mathrm{A} + K_\mathrm{A}M_\mathrm{A} + L_\mathrm{A}M_\mathrm{A} - 2(K_\mathrm{A} + L_\mathrm{A} + M_\mathrm{A}) + 4] \tag{3}$$

The surface areas of species B and C can be expressed in similar manner in terms of their respective Bohr radii. In classical probability it is necessary that $(\sigma_\mathrm{A}, \sigma_\mathrm{B}, \sigma_\mathrm{C})$ are integers. A physical interpretation to the present situation (as suggested by these definitions) could be that instead of the points being paired off as anticipated in the introduction to our problem we now have 'little squares' or area elements to be paired off. The reason for going from points to 'tiles' lies in the discrete (and finite) nature of classical probability. Surfaces scale in a fractal manner, but we restrict the description to rhombi with flat faces. Also note that the number density N_A and the dimensions K_A, L_A and M_A are functions of time.

2.2. Probability of A/B contact

From now on we use the following convention: The letters A and B denote surface area of reactant particles of species A and B such that $B \geq A \geq 0$. Likewise C

[1] Mathematically speaking the domain which consist of the surfaces of all particles are bijectively mapped onto itself where the identity mapping is prohibited.

[2] Where $x \neq y \neq z$.

[3] Scaled radius is the side of a cube that contains an atom, instead of a sphere.

denotes the surface area of product particles. In other words, $A = \sigma_A$ if $\sigma_A \leq \sigma_B$, otherwise $A = \sigma_B$. This convention is advantageous for the calculation of the probabilities. Let $\Gamma = A + B + C$ hence Γ is the sum of all the tiles that must be mapped. Using classical probability and the assumption of ideal mixing as defined, the fraction of the total area-on-area ($\Gamma/2$) that is A on B is computed. We would like our solution to be 'unit free' (and hence unique) and it is accomplished by shrinking the squares into points. If one defines the dimensionless areas: $a = (A/\Gamma)$, $b = (B/\Gamma)$ and $c = (C/\Gamma)$ one is able to express A as $a\Gamma$ and mathematically execute the 'shrinking' by letting $\Gamma \to \infty$. Hence, in the final analysis we find that what really matters is the (dimensionless) fractions a, b and c with the limit $\Gamma \to \infty$ being wholly independent of units as the reader can verify.[4] To summarize, our strategy is to first solve the problem for a finite discrete situation, i.e. given a and b ($c = 1 - (a + b)$) and the parameter Γ, determine the fraction of $\Gamma/2$ that is A on B? Then we take the limit $\Gamma \to \infty$ to obtain the unique unit free solution.

The number of distinct ways that G can be paired is $(\Gamma!/(0.5\Gamma)!)0.5^{\Gamma}$.

$\Gamma!$ presents all permutations, divided by $[0.5\Gamma]!$ since the 'order of the pairs' does not matter and the final term reflecting the fact that for our purposes the order within a pair does not constitute a unique event. Also note that Γ must be even, a condition that becomes irrelevant when Γ becomes large. This is an expression for the total of all possible distinct events. Before we proceed we need to introduce one more definition. Let $Z \geq 0$ be the number of desirable A–B pairs. Using the same principles as before we are now ready to calculate for any integer Z the number of A–B pairs. And then, by taking the fraction of the total as already calculated we can determine the probability that there will be Z A–B pairs. It is obvious that the probability will be zero unless $Z \leq A$. For all $0 \leq Z \leq A$, using the same reasoning as before, the probabilities for gaseous and condensed products, respectively, are

$$P(Z,A,B) = \frac{1}{Z!}\frac{A!}{[(A-Z)/2]!}\frac{B!}{[(B-Z)/2]!}\frac{[\Gamma/2]!}{\Gamma!}2^Z \quad \text{when} \quad C = 0 \tag{4}$$

and when $C > 0$ ($A + B < \Gamma$)

$$P(Z,A,B,C) = \frac{A!}{Z!}\frac{B!}{[B-Z]!}\frac{[\Gamma/2]!}{\Gamma!}2^Z \times \sum_{k=0}^{\Delta}\frac{1}{k'!}\frac{1}{[(A-Z-k')/2]!}\frac{C!}{[C-k']!} \times \frac{[(B+C)-(Z+k')]!}{[((B+C)-(Z+k'))/2]!}2^{k'} \tag{5}$$

where $\Delta = (\min(A - Z, C))/2$ and $k' = 2k$ when Z is even or $\Delta = (\min(A - Z - 1, C - 2))/2$ and $k' = 2k + 1$ when Z is odd.[5]

These formulas yield typical probability distribution curves for given A, B and C situations as shown in Fig. 1. Although a tile of type A cannot map onto another tile A that is right next to it, because they belong to the same particle, for a large number of particles the error becomes small for permitting this type of mapping. To illustrate Eq. (5), first consider the problem of 100 tiles, consisting of 20 tiles of type A, 30 of type B and the balance of type C. The curve $D = P(Z, 20, 30, 50)$ plots the probability to have Z pairs of A–B. The highest probability of 20% is found for 6 pairs of type A–B. It is also clear that the probability to have 10 or more pairs is extremely small. However, $Z = 6$ is not necessarily the most likely outcome. When a total of 120 tiles are considered, $A = 30$, $B = 40$ and the balance C, the highest probability drops to 15% for 13 pairs, shown in curve $E = P(Z, 30, 50, 40)$. The expectancy value is the most likely Z value that one would find. It is akin to taking an expectation value (by integration) when one has a continuous probability distribution and leads to our main result.

2.2.1. Main result

The main result of this study is the expectancy value, given by

$$\Psi(a,b,\Gamma) = \frac{2\sum_{Z=0}^{A} ZP(Z,a,b,\Gamma)}{\Gamma} \tag{6}$$

[4] Those familiar with more modern probability theory might observe that the problem can be formulated in the language of functional analysis but solving it would require 'a measure over the operator-space of all bijective mappings of Γ onto itself'. If this does not sound bad enough already consider that this operator space we envision is likely to be unbounded and nonlinear, and all this would only make sense after adopting some topological labeling over the (expanding) domain making it into a vector space. (A vector space with no necessary physical meaning.)

[5] Consider 0 as even.

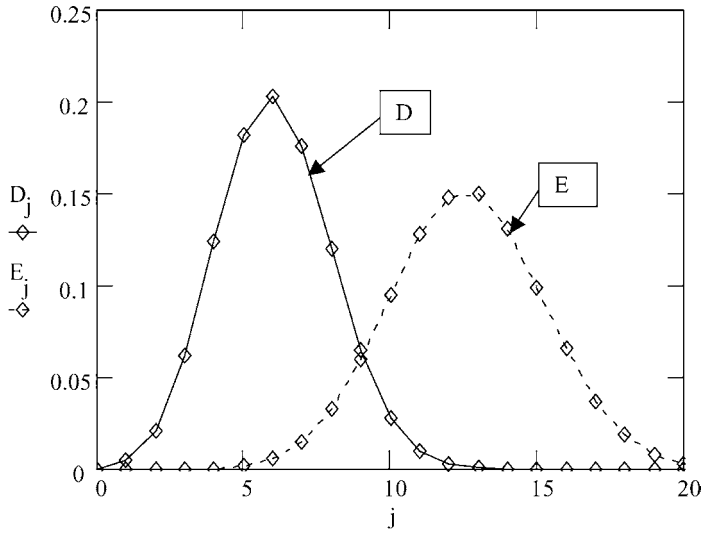

Fig. 1. $P(Z, A, B, C)$ vs. Z.

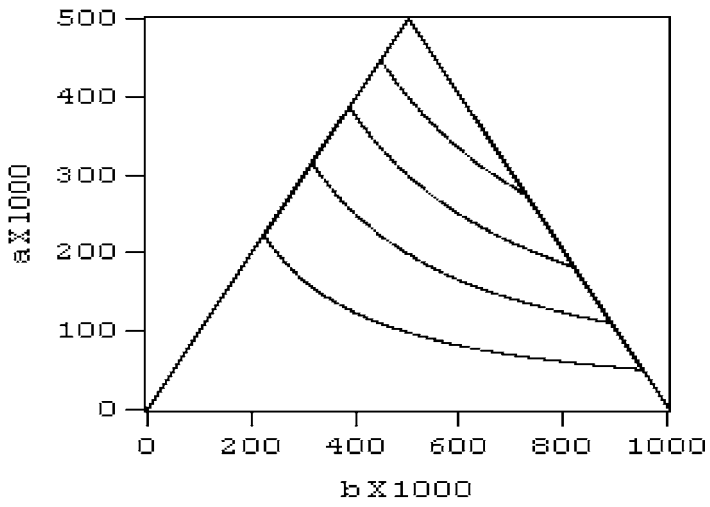

Fig. 2. Expectancy values.

where $P(Z, a, b, \Gamma)$ is given by Eq. (5) and it is expressed as a fraction of the total contacts $\Gamma/2$. Eq. (6) can be applied to any three phase problem to determine the expected fraction of all contacts that would be of type A–B.

Having found this function one can generate a dataset $\Psi(a, b, \Gamma)$ and ideally we would take the limit $\Gamma \to \infty$ but in practice Γ's magnitude would be limited by CPU time. However, as Γ becomes larger, Ψ approaches the limit that is independent of Γ. In Fig. 2 $\Psi(a, b)$ is shown for $\Gamma = 1000$. Note that Ψ reaches a maximum when $a = b$, i.e. $\sigma_A = \sigma_B$ and it is zero when a and/or b becomes zero. It is convenient to display the expectation values on the triangular domain given by the restrictions $a + b \leq 1$ and $b \geq a$ with c implied.[6] As a chemical reaction proceeds, a and b values change. These changes are due to consumption of particles and also other factors like

[6] Since $a + b + c = 1$.

fracture and compression. If one keeps track of these changes, it is possible to map a locus $(a(t), b(t))$ on the $\Psi(a, b)$ surface. The closer the locus remains to the maximum expectancy (region where both a and b are near 0.5), the faster the reaction would be. Low expectancy values could be a result of small available surface area of either reactant or the interference from product. The locus may possibly start at the right (somewhere on the line $a + b = 1 \Rightarrow c = 0$) if there is initially no product and possibly ending in or close to the point $a = b = 0$ if the reaction goes to completion and the reactant mixture has been stoichiometric.

2.3. Reaction rate

The expectancy value must be combined with the total solid surface area and energy distribution to formulate the reaction rate. It is assumed that the atoms at A/B contacts are in thermal equilibrium. They oscillate in their potential wells with certain frequencies and occasionally they occupy the higher end of the Boltzmann distribution and then they are able to cross the activation energy barrier. The reaction rate can be formulated as: rate = concentration A/B contacts × fraction of these concentrations that have more than activation energy × frequency of oscillations in potential well. The concentration of A/B contacts follow from Eqs. (3) and (6)

$$C_{\mathrm{AB}} = \Psi \times \frac{(\sigma_{\mathrm{A}} + \sigma_{\mathrm{B}} + \sigma_{\mathrm{C}})}{2} \tag{7}$$

and it can be divided by Avogadro's number to find the molar density. If the frequency of oscillation is associated with the Debye frequency ν_{D}, the rate expression becomes

$$r = k_0(\nu_{\mathrm{D}}) C_{\mathrm{AB}}\, \mathrm{e}^{-E/RT} \tag{8}$$

The standard model for solid–solid reactions consists of a species balance for each component (or one less species balances and an overall continuity equation), momentum balances, energy balances and an EOS[7] for every species. Quite often the momentum balances are dropped, because the particles are stationary, but they must be included in the general description. However, the system is not closed, since the reaction rate of Eq. (8) requires information about the surface area densities σ_i of all species. The surface area density can change due to changes in the particle number density N_i and the dimensions (K_i, L_i, M_i) (cf. Eq. (3)). The processes that influence surface area density are as follows.

2.3.1. Convection of particles

The convection can be modeled by the standard conservation equation, it describes how particles are advected by macroscopic flow. Particle convection of zero porosity systems occurs under shock. Usually the material is above its Hugoniot elastic limit.

2.3.2. Fracture[8]

Fracture is such a complex process that a fundamental description is still lacking. We resort to an empirical criterion that has been verified experimentally, the Hiramatsu–Oko equation:

$$P l_{\mathrm{A}}^2 = R_{\mathrm{A}} \tag{9}$$

where $P(\bar{x}, t)$ is the pressure, l_{A} represents a dimension of the particle and R_{A} is a material property. In experimental studies Shipway and Hutchings [26] and Sikong [27] consistently find that applied pressure relates to spherical particle diameter according to this relation. The assumption in this work is that this equation also applies to a rhombus. The three dimensions $(K_{\mathrm{A}}, L_{\mathrm{A}}, M_{\mathrm{A}})d_{\mathrm{A}}$ are compared to l_A. For example, if $L_{\mathrm{A}} > l_{\mathrm{A}}$, the rhombus is broken exactly in half along that dimension to form two particles with dimensions $(K_{\mathrm{A}} \times (L_{\mathrm{A}}/2) \times M_{\mathrm{A}})$. If any of the other dimensions would exceed the Hiramatsu–Oko criterion, the fracture process would occur again to form more of the smaller particles. Fracture changes the particle number density and the surface area.

The discontinuous nature of these breaking events implies that classical solutions would cease to exist at the first breaking event. Yet between breaking events the whole system of equations could still be well behaved. Therefore it is mathematically expedient to view the problem as follows: At time t the system is well defined with all conditions known. At some later time t_1 a breaking event occurs. At this moment

[7] For a multi-component system like ours the EOS is not a single equation but rather a system of equations consisting of the individual EOSs of all components and modeling assumptions like assuming a single pressure ($P = P_{\mathrm{A}} = P_{\mathrm{B}} = \cdots$ at x) and temperature (local equilibrium) at every x.

[8] Of course we are assuming $T < T_{\mathrm{melt}}$.

we 'jump' to a 'new' problem/system by carrying over all the variables like $T(x, t_1)$, $P(x, t_1)$, $v(x, t_1)$ at t_1, etc. as initial values for the new problem with the exception of N_A, N_B or N_C. Fracture would imply a doubling of the particle number density of A, B or C at the breaking point.[9] Hence, the system would evolve smoothly between breaking events with these events causing 'discrete jumps' to 'new' systems. It has been tacitly assumed that the breaking process occurs instantaneously.

2.3.3. Reaction

The different surfaces of a rhombus react at the same rate, hence chemical reaction changes the dimensions of a particle, but it does not alter the aspect ratio.

2.3.4. Compression

The pressure in the bed may change due to thermal expansion, density differences between products and reactants and external mechanical loading. As a consequence the material density may change. It is usually assumed that mechanical equilibrium holds between different species (pressure in A, B or C is the same) and material densities could be assessed from the respective EOS. In this study the Shchetinin equation [28] for cold compression (elastic component) is combined with linear thermal pressure:

$$P(\overline{x}, t) = \frac{K_{T_0\mathrm{A}}}{\chi}\left[\mathrm{e}^{\chi(1-v/v_0)} - 1\right] + \alpha_{\mathrm{TA}} K_{T_0\mathrm{A}}(T - T_0) \tag{10}$$

This effect plays a secondary role, compared to convection and reaction. But this effect is more pronounced when reactants have significantly different compressibility properties (K_{T_0}, χ).

The volume per particle is calculated from the particle density (effected by convection and fracture), the material density (effected by compression) and bed density (effected by convection and reaction) as follows:

$$N_i \rho_i v_i = \rho_{\mathrm{Bi}} \tag{11}$$

After the total volume change $v_i(t + \delta t) - v_i(t) = \Delta_{\mathrm{TA}} = \Delta_{\mathrm{rA}} + \Delta_{\mathrm{cA}}$ has been calculated the final step would be to relate it to the changes in (K_i, L_i, M_i) for species i. One option would be a symmetry assumption like $\Delta K = \Delta L = \Delta M$. It is easy to verify that given a total change Δ_{TA} all sides shrink/grow[10] by Δ_{m} where Δ_{m} satisfies the cubic equation

$$(\Delta_{\mathrm{m}})^3 + (K_{\mathrm{A}} + L_{\mathrm{A}} + M_{\mathrm{A}})(\Delta_{\mathrm{m}})^2 + (K_{\mathrm{A}}L_{\mathrm{A}} + K_{\mathrm{A}}M_{\mathrm{A}} + L_{\mathrm{A}}M_{\mathrm{A}})\Delta_{\mathrm{m}} = \Delta_{\mathrm{TA}} \tag{12}$$

Strictly speaking the root must be an integer, but we have rounded to the nearest integer in this study.

In summary, it is necessary to track (average) particle number densities and particle dimensions in addition to species, momentum, energy balances and EOSs to close the system when the reaction rate depends on surface contacts. Admittedly these are rudimentary steps towards the resolution of a complex problem but it advances existing models, offers insight into the physical processes and identifies areas of future research. The use of population balances has been avoided in this study by the use of averages. Averages may represent a poor substitute for distributions but the gain in information must be weighed against the extra computational task to solve the integro-differential equations.

3. Illustratory example

It is necessary to track the particle number density and dimensions of all particles, because Γ must be calculated at each point in the reactor (the sum of all surface area densities) before $\Psi(a, b)$ can be evaluated. The formation of C particles depends on the specifics of the mechanism. For example, C could remain between A–B contacts and form a growing layer. In this case the rate could become diffusion-controlled and mass transport by either A or B through the product layer becomes the determining step. Although this mechanism is rather common, it will

[9] The mathematically rigorous might correctly observe that classical solutions will still not exist due to the spatial discontinuities that may exist in the functions $NP(x)$. The smoothness of $P(x)$ though ought to keep these discontinuities from becoming problematic from a numerical or calculational point of view. The mathematical purist though might resolve the situation by introducing the breaking event increases not pointwise but rather by some decaying smooth distribution around the breaking point.

[10] That is $\mathrm{d}m^{\mathrm{new}} = \mathrm{d}m^{\mathrm{old}} + \Delta m$, $\mathrm{d}n^{\mathrm{new}} = \mathrm{d}n^{\mathrm{old}} + \Delta m$ and likewise for $\mathrm{d}t$.

require that the expectancy value be calculated only once at the onset of the reaction. If condition exists that could lead to fracture, the treatment of the diffusion layer becomes difficult. But we would like to demonstrate the effect of contacts under different, competing conditions. For these reasons it has been decided to choose another mechanism to illustrate the application of the combinatorial approach. This mechanism is based on the assumption that the newly formed product C does not form a layer on A or B. But they could enlarge existing C particles or form new C particles. It is known that beyond a critical size, new particles become stable. This critical dimension enters the model as an additional parameter (since the critical dimension is a scalar, product particles form as cubes in this model). In this mechanism the rate-determining step does not switch over to a diffusion mechanism, therefore the inhibiting effect of C on the true kinetics can be demonstrated.

To simplify the system further, the initial powder charge is placed in an adiabatic container with rigid walls (constant total volume) and heated uniformly. Although the initial pressure of the system can be varied, shocks are not applied, particle velocities are zero and therefore the major simplification is that no thermal or momentum gradients exist between different points in the system. The initial data are provided. The algorithm for the general case simplifies for the batch system as follows. It is explained as an explicit discrete integration procedure.

1. Using initial data, calculate σ_i from Eq. (3), Γ and $a = (\sigma_A/\Gamma)$, $b = (\sigma_B/\Gamma)$. Find $\psi(a, b)$ and solve for r from Eqs. (7) and (8).
2. Calculate bed densities $\rho_{Bi}(t + \delta t)$ from species balances.
3. Calculate temperature $T(t + \delta t)$ from internal energy balance.
4. Calculate material densities $\rho_i(t + \delta t)$ by equating any two of the EOS's to the third one (mechanical and thermal equilibria between phases) and solve them together with the conservation equation: $\sum_{i=a,b,c}(\rho_{Bi}(t + \delta t)/\rho_i(t + \delta t)) = 1$.
5. Check for breaking. If any side of the average particle ($i = a, b, c$) exceeds the breaking criterion: $K_i(t), L_i(t), M_i(t) > \sqrt{P(t + \delta t)/R_i}$ then the side is halved. Suppose $L_A(t)$ meets the criterion, then $L_A(t + \delta t) = 0.5L_A(t)$. Each time a side meets the criterion, the particle number density doubles.
6. Calculate particle volumes of A and B from Eq. (11): $v_i(t + \delta t) = \rho_{Bi}(t + \delta t)/[N_i(t + \delta t)\rho_i(t + \delta t)]$.
7. Calculate changes in particle dimensions from Eq. (12). Update dimensions of A and B. $K_i(t + \delta t), L_i(t + \delta t), M_i(t + \delta t) = K_i(t + \delta t) + \Delta_i$, $L_i(t + \delta t) + \Delta_i, M_i(t + \delta t) + \Delta_i$.
8. Calculate the number of C molecules formed during $t \rightarrow t + \delta t$ using r; Δ_C.
9. Assign Δ_C between existing C particles and formation of new C particles. For the purpose of this example, the fraction $c = \sigma_C/T$ of Δ_C is assigned to existing particles. The remainder forms new particles of the specified critical dimensions; $\Delta N_C = (1 - c)\Delta_C/[L^3_{crit}]$. This creates two different particle sizes for C. The existing particles and the newly formed particles are summed to find the updated $N_C(t + \delta t)$. The average particle volume is found from Eq. (11): $v_C(t + \delta t) = \rho_{BC}(t + \delta t)/[N_C(t + \delta t)\rho_C(t + \delta t)]$ and since C particles are cubic, the updated dimension can be easily determined.
10. Time is updated and return to step 1 for next integration step.

The reaction that is considered in this example is: $A + 4B \rightarrow C$ and the parameters are listed in Table 1. Where the parameters have been changed to investigate their influence on the overall reaction rate, the values are stated in the text.

3.1. Breaking properties

In a stoichiometric mixture, moles of species A are less than moles of species B. But this does not mean that σ_A is four times less than σ_B, because surface area also depends on particle size and aspect ratios. However, the parameter values for the base case indicate that the A particles are larger than the C particles and the expectancy value will be strongly influenced by the deficiency in available surface area of A. Therefore, any mechanism that increases surface area of A will cause an increase in the reaction rate. In Fig. 3 the reaction rates are plotted as function of time (scaled by k_0). The fracture parameter R_i has been decreased by factor 10 for A and B in plots 1 and 2, respectively.

Table 1
Parameter values

Property	Default value
E	10^5 J/mol
$K_{T_0\mathrm{A}}$	80×10^9 Pa
$K_{T_0\mathrm{B}}$	60×10^9 Pa
$K_{T_0\mathrm{C}}$	90×10^9 Pa
L (scale for length)	10 μm
$\rho_{\mathrm{A}0}$	2300 kg/m^3
$\rho_{\mathrm{B}0}$	2100 kg/m^3
$\rho_{\mathrm{C}0}$	2450 kg/m^3
C_{vA}	11.35 J/K mol
C_{vB}	8.581 J/K mol
C_{vC}	53.764 J/K mol
$-\Delta H$	58620 J/mol
k_{mixture}	31.35 W/m K
k_0	10^9 s^{-1}
T_0	298 K
R_{A}	5×10^8 MPa μm^2
R_{B}	2×10^8 MPa μm^2
R_{C}	10^9 MPa μm^2
$K_{\mathrm{A}}(0)$	800 μm
$L_{\mathrm{A}}(0)$	700 μm
$M_{\mathrm{A}}(0)$	700 μm
$K_{\mathrm{B}}(0)$	1100 μm
$L_{\mathrm{B}}(0)$	800 μm
$M_{\mathrm{B}}(0)$	400 μm
L_{crit}	0.3 μm
$P(0)$	500 MPa
α_{TA}	6.6×10^{-6} K^{-1}
α_{TB}	5.1×10^{-6} K^{-1}
α_{TC}	7.0×10^{-6} K^{-1}
$d_{\mathrm{A}} = d_{\mathrm{B}} = d_{\mathrm{C}}$	4.0 Å
χ_{A}	5.1
χ_{B}	6.1
χ_{C}	5.1

The initial reaction rate for plot 1 (P1, i.e. A more brittle) is three times higher than for P2 (B more brittle). At this stage the reaction is kinetically controlled since the initial temperature is only 700 K. P1 heats up faster and at its maximum the rate is nearly six times faster than P2. The reaction goes to completion in approximately half the time of P2. This result indicates that solid reaction in the presence of high mechanical loading favors a system where the reactant species with the smaller stoichiometric coefficient fractures more readily.

In Fig. 4 the loci on the expectancy surface are shown. Both P1 and P2 start on the line $a + b = 1$, because $c = 0$. The A particles experience fracture at $t = 0$, hence σ_{A} increases rapidly and the expectancy value lies near the apex that also marks the maximum expectancy value. The spacing between symbols on each plot indicates consecutive time steps, thus the rate can be inferred from it. The kinks in the plots are the points where fracture has occurred. The P1 locus proceeds towards the complete conversion point $(a, b) = (0, 0)$ along a trajectory that lies close to the $a = b$ side, but this side is the optimal trajectory to maximize ψ. In contrast the P2 locus proceeds close to the $a = 0$ side that constitutes small expectancy values and therefore smaller reaction rates. The probability for A–B contacts is small due to the abundance of B surface area (i.e. B–B contacts dominate). Another interesting feature is observed when the complete conversion point is approached (spacing between symbols is getting smaller). The surface area of C becomes dominant and the probability for A–B contacts becomes slimmer for both P1 and P2.

3.2. Initial particle sizes

The reaction rate depends on the product of the expectancy value $\psi(a, b)$ and the total surface area Γ. In Fig. 5 the loci are shown for two mixtures that only differ in the initial particle sizes of both reactants. The locus P1 denotes the base case with all parameters as listed in Table 1. The initial particle dimensions of A and B have been reduced by factor 10 for the locus P2. Because the particle sizes of P1 exceed the breaking criterion, they have fractured (A and B fractured at $t = 0$), hence the surface areas ratios have remained the same and both loci start at the same point on the surface. However, the particle sizes of P2 are smaller than P1 and the reaction rate is higher, compare the spacing between symbols for P2 and P1. As the reaction proceeds, the pressure increases, this is largely due to thermal expansion. Although the particles of P1 have fractured initially, they are still larger than the particles of P2. The further kinks in the P1 locus indicate more breaking events as the pressure increases. But the particles of P2 have never met the breaking criterion. The P2 locus reaches the complete conversion point in far fewer time steps than P1. Compression plays here a minor role in the expectancy value, but particle consumption by reaction is quite important. The P2 locus does not experience fracture and it is a straight line between

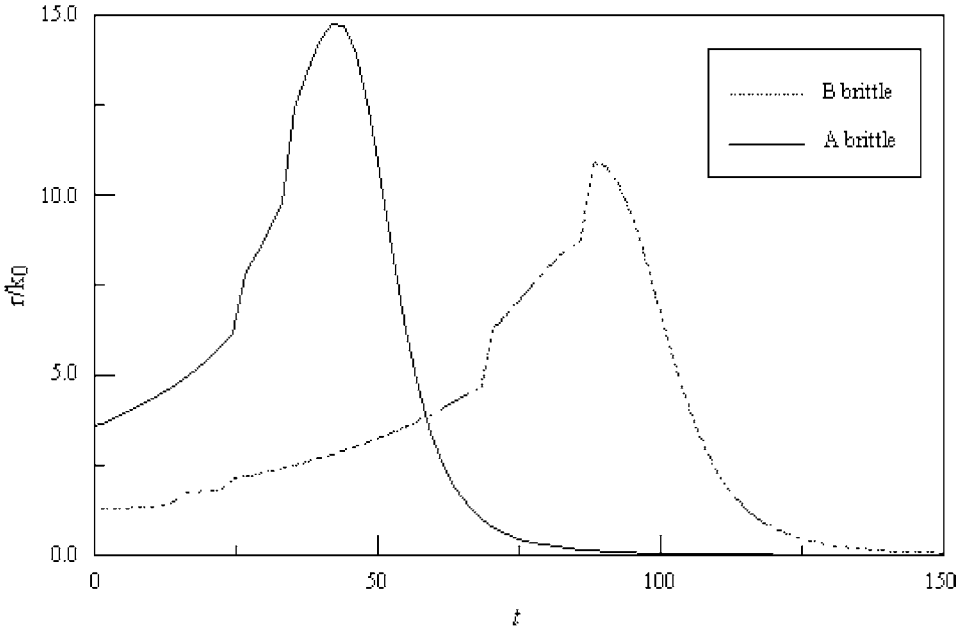

Fig. 3. Comparison of different fracture conditions.

the starting point on the line $a + b = 1$ and $(a, b) = (0, 0)$.

In the following study the fracture criteria have been adjusted upwards to avoid any possible fracture. Both A and B particles are cubes of the same dimensions and preheated to 800 K. Further temperature rise is due to the chemical reaction. The reaction rates (cf. Eq. (8)) are shown for cubes of 5 and 10 μm, 50 and

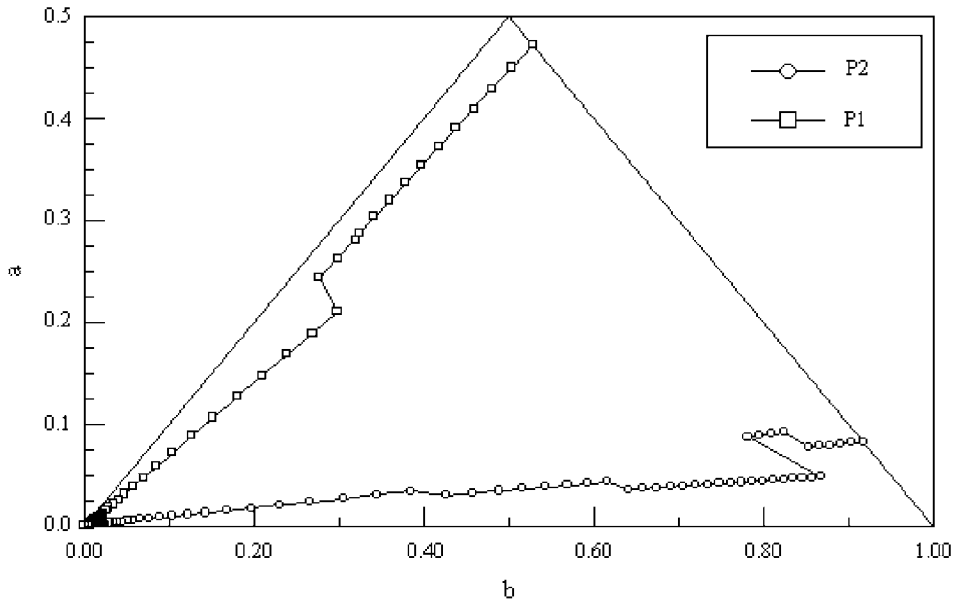

Fig. 4. Reaction locus on expectancy surface.

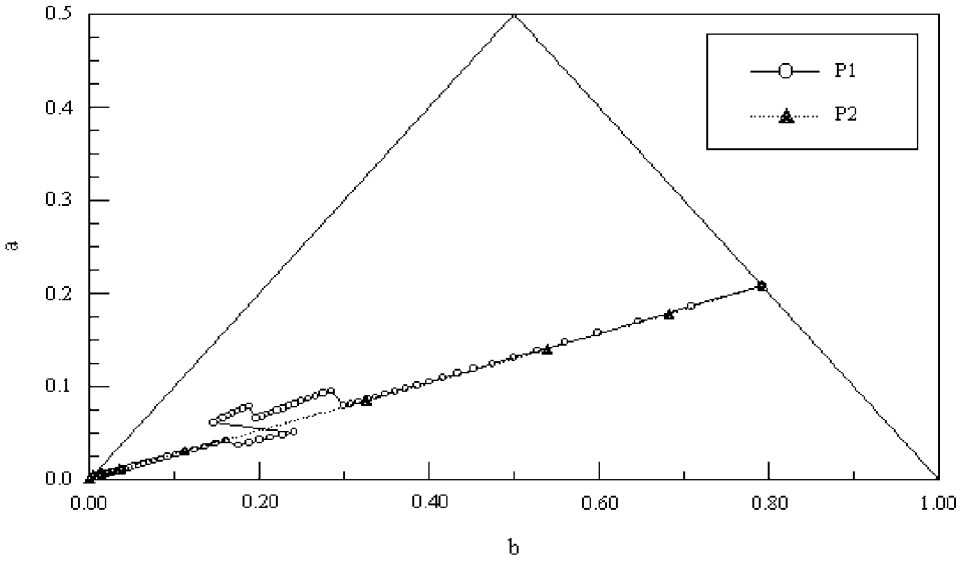

Fig. 5. Reaction loci for different particle sizes.

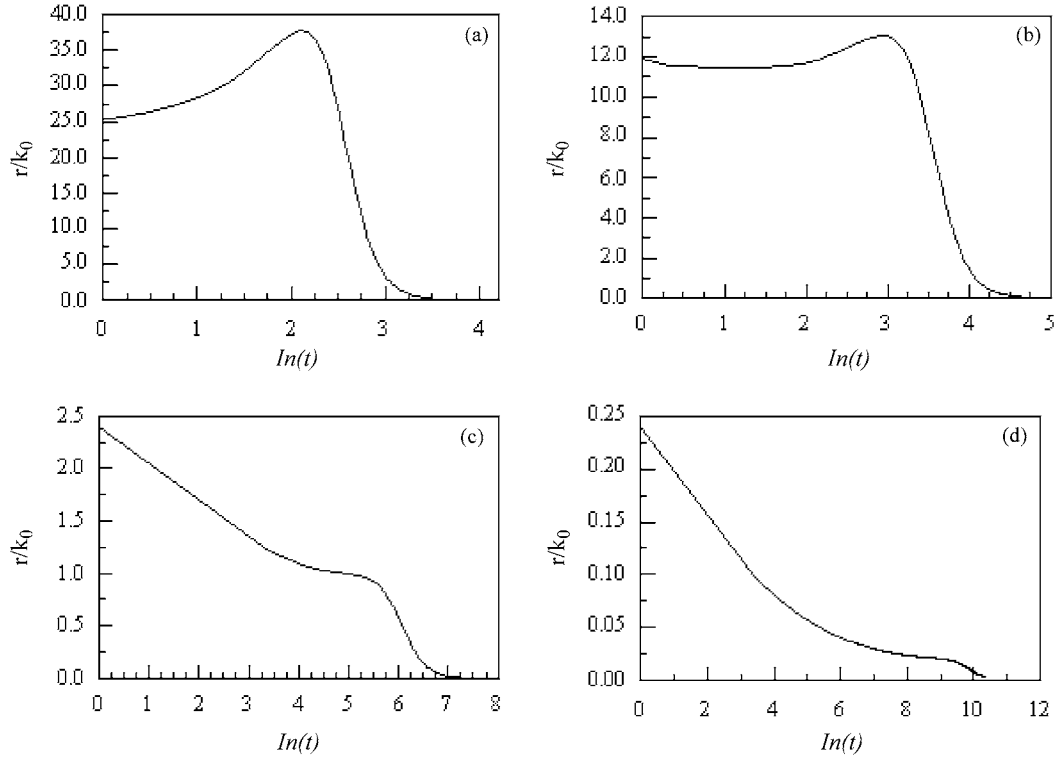

Fig. 6. Reaction rates for different initial particle sizes.

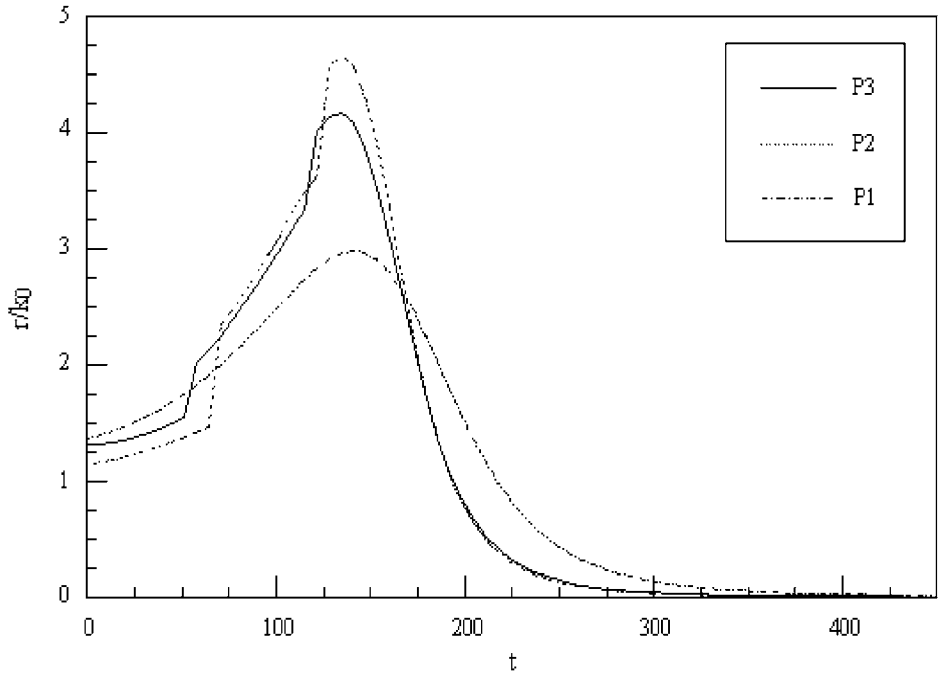

Fig. 7. Reaction rates for different particle geometries.

500 μm in Fig. 6a–d. The reaction rates exhibit three different forms. When the particles are 5 μm, the reaction rate is fast, the temperature increases rapidly and the overall rate increases from the onset. The local maximum presents the point where $C_{AB} = \Psi(\sigma_A + \sigma_B + \sigma_C)/2$ becomes rate controlling. The reaction is complete in 35 time units (scaled by k_0). When the particle size is doubled, the reaction rate decreases slightly in the beginning, then it increases and reaches a local maximum before the rate drops of finally. This competition between the decreasing effect of C_{AB} and the increasing effect of temperature on the overall rate is shown in Fig. 6b. Complete conversion is achieved after $t \approx 10$. The reaction rate for the 50 μm particles (Fig. 6c) decreases and it is at the maximum at $t = 0$. The rate is controlled by C_{AB} which is a monotonically decreasing function of time. The temperature increases in the adiabatic system and the Arrhenius component becomes larger, causing a slowdown in the decrease, this is noticeable as the quasi-plateau in Fig. 6c. The reaction is complete at $t \approx 1400$. The 500 μm particles react slowly and the reaction is complete after $t \approx 36\,000$. Progressively increasing the particle dimensions leads to a point where the local minimum, maximum and the inflection point coincides and beyond that the reaction rate becomes monotonically decreasing. This is illustrated in Fig. 6c and d.

3.3. Geometry

The geometry has been investigated by comparing the reaction rates for three different mixtures: (a) all particles are cubes, (b) A particles have aspect ratio 1:3:8 and B particles are cubes and (c) A particles are cubes and B particles have ratio 1:3:8. (The rhombi have the same volume as the cubes in all cases.) In Fig. 7 the reaction rates are plotted for cases a, b and c as P1, P2 and P3, respectively. For a short period after onset, P1 is largest. This is a result of fracture. The cubes fracture to generate eight particles from each cube, the initial rhombus dimensions only exceed fracture criterion along two sides, thus generating four particles per rhombus. P1 does not experience further fracture, but P2 and P3 fracture more to generate further surface area. Eventually P2 and P3 exceed P1.

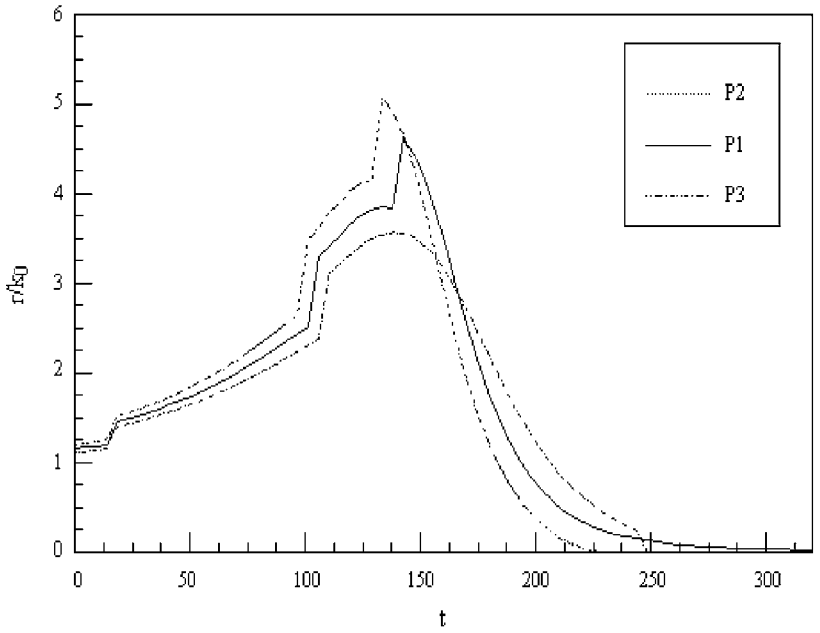

Fig. 8. Reaction rates for different stoichiometry.

3.4. Mixtures and stoichiometry

The last parameter that is investigated is the stoichiometry of the mixture. The stoichiometry is changed from 1:4 to 1:3.5 to 1:4.25 in plots P1–P3 of Fig. 8, respectively. The expectancy value is raised when the surface area of A is increased, therefore the reaction rate of P2 is the fastest. When more B is added, the probability for A–B contacts is reduced and P3 is the smallest of all the rates. However, as the other two rates approach completion (i.e. P1 and P2), interference by C actually reduce those rates below that of P3. Although P3 proceeds slower than P1 for most of the time, full conversion of the limiting reactant A is accomplished in less time. In P2 and P3 the reaction only goes to completion in B and A, respectively. The interesting point that comes out of this study is that reaction rates can be accelerated by shifting mixture composition towards higher concentrations of the component with smallest stoichiometric coefficient.

4. Conclusions

A combinatorial method has been proposed to determine statistically the expected number of successful contacts in a three-phase system. It is necessary to track surface densities of all three solid phases. The evolution of surface density is affected by several factors. The exact description depends on the mechanism and an example has been presented where particle consumption by reaction, compression, fracture and product precipitation have been considered. But it must be understood that the combinatorial result stands apart from the mechanism, it becomes an additional variable in a more detailed macroscopic description. It is the evaluation of the expectancy value that necessitates the expansion of the set of governing equations to particle sizes and dimensions. Of course, the treatment of particle sizes as distributions would greatly increase the level of information, but the computational burden will also go up. Including $\psi(a,b)$ in the kinetics does not merely bring particle sizes neatly into the kinetic expression, but particle geometry and stoichiometry become implicitly part of it as well.

The methodology to include $\psi(a,b)$ has been demonstrated for a specific mechanism. Parameters have been varied and all the trends that have been observed are consistent with the competition that exists between contacts and the factors that influence

the outcome of successful contacts. Any process that increases the surface area density of the minority species that participates in successful contacts would lead to an enhancement of the reaction rate. If an increased reaction rate is the objective, it could be accomplished in a variety of ways, as demonstrated in the example. Reducing the particle size of the minority species, large aspect ratios and non-stoichiometric mixtures shifted towards higher concentration of the minority species all contribute towards higher reaction rates. These parameters offer some flexibility to adjust reaction rate for a specific chemical system. Generally systems are not mechanically loaded to induce fracture, but there is a growing awareness of the important role of mechano-chemical coupling. Mechano-chemical coupling encompasses many affects, but fracture is definitely one of them.

Experimental verification of these findings will be very valuable. Once the experimental system has been selected, the specific mechanism must be determined. It is necessary to know the mechanism in order to track the evolution of product species. The contact area is determined at the onset of the reaction. The prevailing conditions in the reactor will dictate the necessity to calculate the expectancy value once at the beginning of the reaction (no further mixing after ignition), or continuously (mixing occurs while reaction proceeds). A particularly interesting experiment can be proposed to investigate the effect of aspect ratio. If cubes (or spheres), platelets and needles of the same reactant are compared in three separate experiments, with careful consideration of the initial porosity, it will be possible to lend credence to, or even verify, the theory.

The next task at hand is to include porosity in a sensible manner. This enters as a fourth species with volume occupied by pores equivalent to the complement of the solid space.

As mentioned earlier, the combinatorial problem for four species is computationally immense. However, a very interesting problem that falls in the scope of the current combinatorial problem would be $A_s + B_s \rightarrow C_g$. The gas phase is treated as the third species and the requirement that the system must be pore-free can be dropped. This work is under way. Another problem that is currently addressed is the common problem of the formation of a product layer between reactants and subsequent diffusion control.

Acknowledgements

The authors acknowledge the financial support of the National Science Foundation through grant CTS-0096381.

References

[1] J.M. Smith, Chemical Engineering Kinetics, McGraw-Hill Publ. Co., New York, 1981.
[2] S.S. Tamhankar, L.K. Doraiswamy, AIChE J. 25 (1979) 561.
[3] A.G. Merzhanov, Comb. Sci. Flame 98 (1994) 307.
[4] A. Varma, A.S. Rogachev, S. Hwang, Adv. Chem. Eng. 24 (1998) 81.
[5] N.S. Enikolopyan, Doklady Akad. NAUK 283 (1985) 612.
[6] N.S. Enikolopyan, A.A. Mkhitaryan, A.S. Karagezyan, Doklady Akad. NAUK 288 (1985) 436.
[7] N.S. Enikolopyan, Russ. J. Phys. Chem. 63 (1989) 1261.
[8] N.S. Enikolopyan, A.A. Mhkitaryan, A.S. Karagezyan, A.A. Khzardzhyan, Doklady Akad. NAUK 292 (1987) 121.
[9] N.S. Enikolopyan, V.B. Vol'eva, A.A. Khzardzhyan, V.V. Ershov, Doklady Akad. NAUK 292 (1987) 177.
[10] N.S. Enikolopyan, A.A. Khzardzhyan, E.E. Gasparyan, V.B. Vol'eva, Doklady Akad. NAUK 294 (1987) 567.
[11] N.S. Enikolopyan, A.A. Mkhitaryan, Doklady Akad. NAUK 309 (1989) 900.
[12] N.S. Enikolopyan, Doklady Akad. NAUK 302 (1988) 862.
[13] N.S. Enikolopyan, A.I. Aleksandrov, E.E. Gasparyan, V.I. Shelobkov, A.A. Mkhitaryan, Doklady Akad. NAUK 319 (1991) 612.
[14] V.F. Nesterenko, M.A. Meyers, L.C. LaSalvia, Metal. Mat. Trans. A 26 (1995) 2511.
[15] V.F. Nesterenko, M.A. Meyers, H.C. Chen, J.C. LaSalvia, Appl. Phys. Lett. 65 (1994) 3069.
[16] H.C. Chen, J.C. LaSalvia, V.F. Nesterenko, M.A. Meyers, Acta Mat. 46 (1998) 3033.
[17] N.N. Thadhani, Prog. Mat. Sci. 37 (1993) 117.
[18] N.N. Thadhani, High Strain Rate Behavior of Refractory Materials, TMS, Warrandale, PA, 1991.
[19] B.R. Krueger, A.H. Mutz, T. Vreeland Jr., J. Appl. Phys. 70 (1991) 5362.
[20] M.B. Boslough, J. Chem. Phys. 92 (1990) 1839.
[21] J.N. Johnson, P.K. Tang, C.A. Forest, J. Appl. Phys. 57 (1985) 4324.
[22] L.S. Bennett, Y. Horie, M.M. Hwang, J. Appl. Phys. 76 (1994) 3394.
[23] L.S. Bennett, F.Y. Sorrell, I.K. Simonsen, Y. Horie, K.R. Iyer, Appl. Phys. Lett. 61 (1992) 520.
[24] T. Vreeland Jr., K.L. Montilla, A.H. Mutz, J. Appl. Phys. 82 (1997) 2840.
[25] Y. Horie, M.E. Kipp, J. Appl. Phys. 63 (1988) 5718.
[26] P.H. Shipway, I.M. Hutchings, Powder Technol. 76 (1993) 23.
[27] L. Sikong, Powder Technol. 61 (1990) 51.
[28] V.G. Shchetinin, Combustion Explosions and Shock Waves 27 (1991) 426.